A Motion-Powered Piezoelectric Pulse Generator for Wireless Sensing via FM Transmission

Hao Jiang, Michail E. Kiziroglou, *Member, IEEE*, David C. Yates, *Member, IEEE*, and Eric M. Yeatman, *Fellow, IEEE*

***Abstract*—A motion-powered pulse generator using piezoelectric transduction is reported in this paper for wireless sensing devices. A metallic rolling ball is implemented in the prototype as an inertial proof mass excited by external motions at random low frequency. Taking advantage of the metallic proof mass, magnetic coupling can be achieved to actuate the piezoelectric cantilever by attaching tip magnets to the free end. In addition, self-synchronous switching is achieved by applying electrodes to the track of the rolling ball. A new passive prebiasing mechanism is introduced to improve the performance of the pulse generator. Both simulation and experimental results were conducted to demonstrate the improvement. Experimental results show that 76% more energy can be extracted by the prebias mechanism compared to the unbiased case. A transmission circuit based on a Colpitts oscillator was built to test the performance of the capacitor-powered oscillator, which is designed as the load of the pulse generator. By adding a voltage control component, the transmission circuit is capable of encoding a sensor signal by frequency modulation, which demonstrates the feasibility of implementing a motion-powered wireless sensing prototype based on the piezoelectric pulse generator.**

***Index Terms*—Energy harvester, piezoelectric energy, pulse generator, wireless sensing.**

I. Introduction

WITH AN increasing demand on smaller electronic devices for body sensor networks and wearable wireless sensing techniques, the maintenance issue of batteries has become a major drawback. For Internet of Things applications, in particular, where electronic functionality is added to very large numbers of autonomous objects, maintenance-free power provision is an essential enabler. Exploring sustainable power sources has become a popular topic, aiming to extend the lifetime and meet the requirement of miniaturized devices [1]. Many approaches, including exploitation of light and temperature differences, have been implemented as power supplies [2], [3]. Ambient motion is another promising energy source that has drawn increasing research interest, and inertial energy harvesters have proved to be an excellent candidate as a power source [4].

A self-powered wireless sensor network (WSN) node platform has been reported by our group using electrostatic transduction [5]. A metallic rolling rod was integrated into the prototype as an external proof mass, such that it could be excited by random low frequency. This prototype converts energy from ambient motions to electrical energy and amplifies it via variable capacitances for wireless transmission. This design demonstrates a new concept for instant wireless sensing using energy harvesting techniques. However, due to the low variable capacitances achievable from electrostatic transduction, the energy extracted from the device is very limited, and only 2 nJ per operating cycle can be harvested.

Piezoelectric transduction has attracted considerable research interest and has been proved as an excellent method in terms of energy generation [6]–[8]. Using the rolling rod as an external proof mass, a piezoelectric energy harvester has been designed [9]; the prototype shows good performance for energy harvesting, but cannot be applied to wireless sensing directly. By combining the features of the two devices in [5] and [9], a rolling ball pulse generator using piezoelectric transduction has been developed and is presented here. This device provides substantial output, which can be applied directly as a power source for its load circuit, so that a motion-powered wireless sensing prototype can be designed based on this device.

The piezoelectric pulse generator consists of two parts, which are: 1) the electromechanical prototype and 2) the intermediate circuit. The electromechanical part is excited by ambient motion, and generates energy via piezoelectric transduction. The circuit part is designed to store a fixed amount of energy and discharge it into the next stage load circuit in each operating cycle.

This paper presents the structure and the operating principle of the pulse generator. Results both from simulations and experiments are provided to demonstrate the performance of the device. A passive prebias mechanism is introduced to enhance the amount of energy extracted in each operating cycle, and is also demonstrated both from simulations and experiments. A capacitor-powered oscillator is designed and tested as the load of the pulse generator, and a frequency modulation approach is added for wireless sensing.

II. Energy Generation From Piezoelectric Transduction

The structure of the rolling ball prototype is presented in Figs. 1 and 2. As illustrated in the figures, the substrate of the device is made of glass plates. A piezoelectric cantilever is allocated under the substrate, and two magnets M_1 and M_2 are attached to the free end of the beam for suitable magnetic strength. A steel rolling ball, which is mounted in the V-groove track of the substrate, is used as an external proof mass and

Manuscript received June 18, 2014; revised October 24, 2014; accepted December 13, 2014. Date of publication December 24, 2014; date of current version February 04, 2015. The authors are with the Department of Electrical and Electronic Engineering, Imperial College London, London SW7 2BT, U.K. (e-mail: hao.jiang10@imperial.ac.uk).

Color versions of one or more of the figures in this paper are available online at http://ieeexplore.ieee.org.

Digital Object Identifier 10.1109/JIOT.2014.2385891

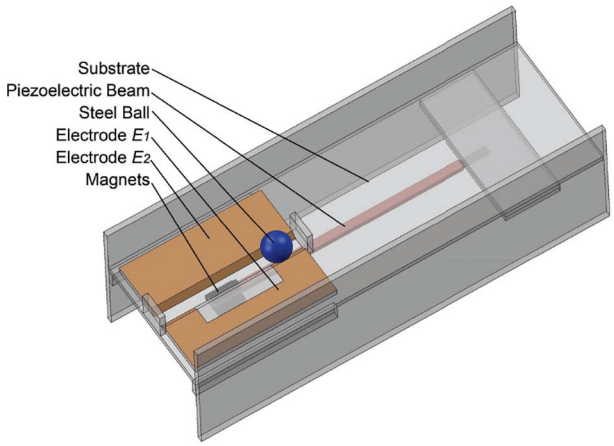

Fig. 1. Electromechanical part of the rolling ball pulse generator.

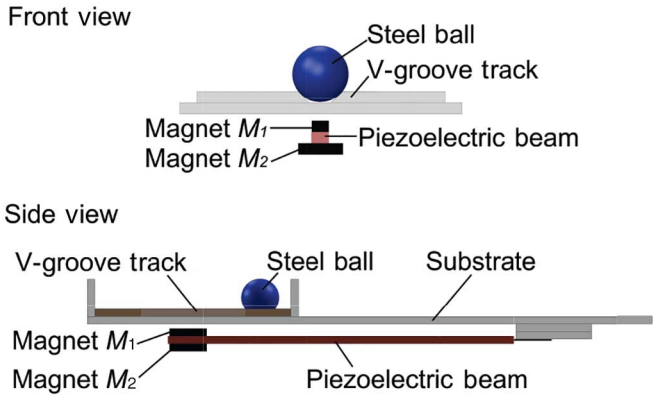

Fig. 2. Section views of the electromechanical prototype.

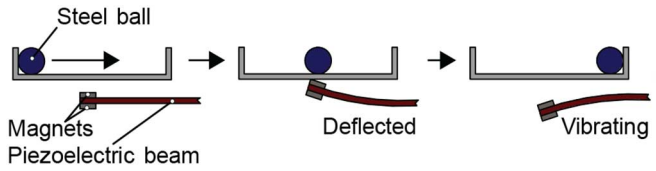

Fig. 3. Operating process when the steel ball travels from one end-stop to the other.

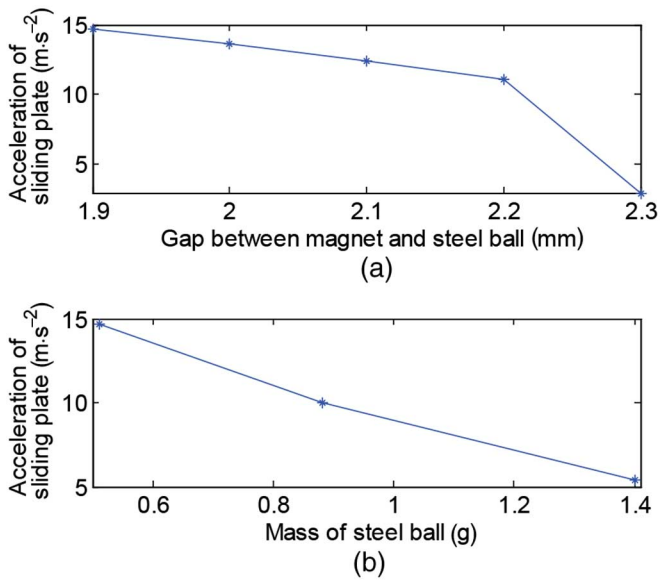

Fig. 4. Dynamic analysis excited by the sliding plate. (a) Minimum external acceleration required to release the steel ball from the magnets with different gaps between the magnet and the ball. (b) Minimum acceleration for the sliding plate with different steel balls.

excited by the motion source. In addition, the metallic rolling ball forms magnetic coupling together with the tip magnets on the piezoelectric beam when it rolls along the track. The electrodes E_1 and E_2 are used as a self-synchronized switch when the prototype is connected to a electrical load.

Piezoelectric energy generation is conventionally analyzed and used under constant base excitation such as in [10]. By applying the external rolling proof mass to the prototype as presented in Fig. 2, the piezoelectric beam can be actuated discontinuously by the magnetic coupling between the metallic rolling ball and the tip magnets. When the device is excited by a reciprocating external motion horizontally (this is provided by a sliding plate controlled by a servo drive from Kollmorgen, on which the device is mounted in the experiments), the rolling ball can travel back and forth from one end-stop to the other through the V-groove track. Fig. 3 illustrates the operating process of the device in each cycle. As shown in the figure, when the ball reaches the middle of the track, the magnetic force between the ball and the tip magnets deflects the piezoelectric cantilever, and after the rolling ball moves away from the tip magnets, the cantilever is free to vibrate. Piezoelectric energy can be generated both from the deflection and the vibration, and this process described above is defined as one operating cycle of this device.

In order to achieve the function described above, the magnetic coupling must be high enough to deflect the piezoelectric beam, and the acceleration of the external motion must be sufficient to release the ball from the magnet. Fig. 4 illustrates the minimum acceleration required for the external motion in different situations.

In Fig. 4(a), a 5-mm diameter steel ball ($\sim$0.5) g is used, and the gap between the magnet and the steel ball is defined as the distance between the bottom of the ball and the top surface of magnet M_1 in Fig. 2 when the beam is deflected. As can be seen from the figure, by increasing the gap, the external acceleration needed is decreased. However, the tradeoff is that the reduction of the gap results in a smaller beam deflection, which reduces the energy generated from the beam. In Fig. 4(b), balls with different weights are used to analyze the impact of the motion on the prototype when the gap is fixed at 1.9 mm, and the minimum acceleration required for external motion is decreased with increasing proof mass, which indicates that the ball with larger weight can more easily escape the magnetic force.

Fig. 5 shows the experimental result from the electromechanical prototype, and the open-circuit voltage in one operating cycle is plotted in this figure. As can be seen from the plot, initially a positive pulse is generated when the beam is deflected. The rest of the resonant waveform is from the vibration of the beam. This output result demonstrates a useful energy harvesting performance similar to the rod proof mass device [9]. However, this electromechanical prototype is not directly suitable as a power supply for signal sensing and wireless transmission, since the output voltage is not rectified. By applying

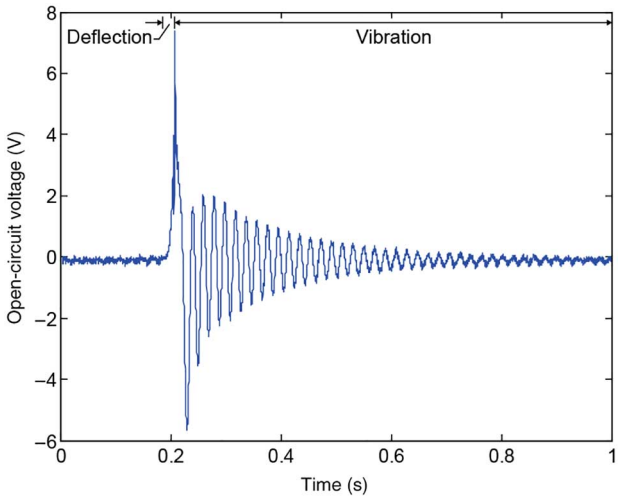

Fig. 5. Open-circuit voltage of the electromechanical part.

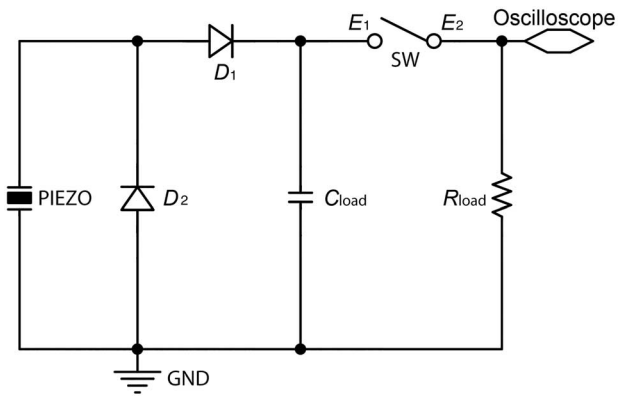

Fig. 6. Schematic of the intermediate circuit.

an intermediate circuit to the prototype, the output energy can be transformed into relatively constant power, which is more compatible with wireless signal processing.

III. Operating Principle of the Pulse Generator: Unbiased Case and Prebiased Case

The schematic in Fig. 6 is the intermediate circuit of the piezoelectric pulse generator. The load capacitor $C_{\rm load}$ in the circuit is the main storage component for the piezoelectric energy from the electromechanical prototype. Two diodes D_1 and D_2 are connected between the piezoelectric element and $C_{\rm load}$, and used as electrical switches for the pulse generator. The switch SW is formed by the two electrodes E_1 and E_2 in Fig. 1, together with the steel rolling ball for self-synchronous switching between the pulse generator and its load.

According to Figs. 5 and 6, when the device is excited by the ambient motion and the rolling ball travels through the track, the positive piezoelectric pulse generated from the deflection makes D_1 forward biased and D_2 reverse biased. This connects the load capacitor $C_{\rm load}$ to the piezoelectric beam and allows $C_{\rm load}$ to share charge with the piezoelectric capacitor.

As the ball travels away from the tip magnet and the beam starts to vibrate, a complicated process occurs while the beam is vibrating. Each time the surface charge of the beam is positive and the voltage potential exceeds the threshold voltage of D_1, $C_{\rm load}$ extracts and stores energy from the vibrating beam. When the surface charge is negative, diode D_2 is forward biased to allow the beam to release the charge and prevent the beam from shifting its electrical neutral axis away from its mechanical neutral axis, i.e., no surface charge is generated when the beam is not deflected. After the energy is stored in $C_{\rm load}$, it can be supplied to the load circuit, via a mechanical switch formed by the rolling ball and the electrodes.

By combining the electromechanical piezoelectric prototype and intermediate circuitry, energy from ambient motions can be transferred to piezoelectric energy and stored into a load capacitor simultaneously. Since the piezoelectric energy is shared between the load capacitor and the piezoelectric beam, only half of the charge can be extracted to $C_{\rm load}$, when the load capacitance is equal to the piezoelectric capacitance. Because the load capacitor can only extracts energy when D_1 is forward biased, most of the extracted energy is from the beam deflection, and losses occurs when the beam is vibrating. In addition, the threshold voltage of the diodes can also introduce losses. These charge penalties reduce the energy extracted in each operating cycle. Therefore, it is worthwhile exploring methods to improve performance.

One method to enhance the amount of energy extracted is to increase the displacement of the piezoelectric beam. However, this is limited by the relationship between the strength of the magnetic coupling and inertial force of the proof mass. A larger tip displacement of the given beam requires stronger magnetic coupling between the tip magnet and the proof mass in order to overcome the stiffness of the piezoelectric cantilever. In this case, when the deflected beam reaches the maximum displacement, an increased magnetic force occurs, and for the given proof mass and acceleration of the ambient motion, the rolling ball may become stuck at the middle of the track if the magnetic force is overly increased. Therefore, the tip displacement is restricted by the mass of the given rolling ball and the ambient motion acceleration availability.

Considering the current prototype, the energy can only be stored into $C_{\rm load}$ when D_1 is forward biased, and therefore most of the energy is extracted from the first positive pulse in Fig. 5. It is important to increase this positive peak amplitude. This can be achieved by prebiasing of the piezoelectric beam without increasing the tip displacement. However, in order to prebias the beam from an external source, such as in [11] and [12], a synchronization circuit is required to prebias the beam only when it is deflected, which causes the design to be much more complicated. Taking advantage of the asymmetric conductance of the diode, a passive prebias method can be applied to this particular prototype to improve the energy extraction rate simply by reversing the polarity of the piezoelectric beam.

When a piezoelectric beam with reversed polarity is applied to the prototype, the deflection of the beam provides a negative surface charge, which makes the diode D_2 forward biased first. This allows the piezoelectric beam to be discharged through D_2 during deflection, and shifts its electrical neutral axis away from its mechanical neutral axis to the maximum tip displacement as shown in Fig. 7. When the rolling ball travels away

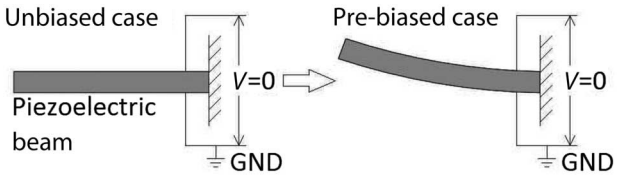

Fig. 7. Passive prebias of the piezoelectric beam.

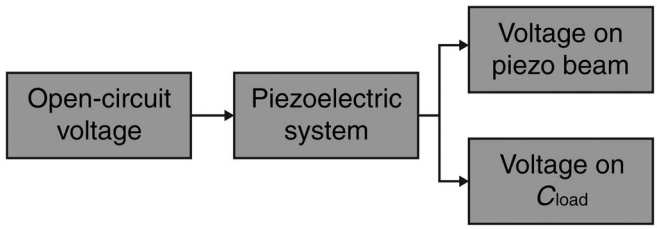

Fig. 8. Architecture of the simulation model.

from the tip magnet, the piezoelectric beam vibrates to the opposing maximum displacement, and provides a higher positive voltage amplitude, which shares more charge with the load capacitor $C_{\rm load}$. This approach was verified both in analytical modeling and experimental results, and the outputs in the unbiased and prebiased case are compared below to demonstrate the improvement.

IV. Analytical and Experimental Models of the Piezoelectric Pulse Generator

In order to demonstrate the feasibility of the piezoelectric pulse generator and the improvement of the prebiased case, an analytical model was built combined with the experimental data in Fig. 5 to simulate the performance of the device in both unbiased and prebiased cases. The prototype based on the structure in Figs. 1 and 6 was realized to test and verify the performance experimentally.

A. Analytical Model for the Unbiased and Prebiased Pulse Generator

Different modeling approaches have been used to analyze the behavior of piezoelectric generators such as [13] and [14]. In order to analyze the process of the presented piezoelectric pulse generation in detail and examine the passive prebiased method to improve the performance, a piezoelectric simulation model based on the current prototype was designed to simulate the charge sharing process when the pulse generator is operating.

The aim of the simulation model is to use the open-circuit voltage measured from the electromechanical prototype to analyze the quasi-static electrical performance of the piezoelectric beam and the load capacitor during operation. Fig. 8 illustrates the architecture of the model. As shown in the block diagram, the open-circuit voltage from the electromechanical part is the input data to the model, and the outputs are the voltages on the piezoelectric cantilever and the load capacitor. This model can be realized because of the linear relationship between the displacement of the piezoelectric beam and the surface charge on it, when it operates in open circuit [15].

In order to simplify the analysis of the quasi-static performance of the piezoelectric beam, a few assumptions are made, which are: 1) the mechanical behavior of the piezoelectric beam is not influenced by the surface charge loss; 2) the piezoelectric beam has no leakage; 3) the capacitance of the load capacitor is equal to the piezoelectric capacitance; and 4) the diodes are assumed as having a finite threshold voltage $V_{\rm th}$ but otherwise ideal. Under the assumptions, the piezoelectric beam has three possible situations when the circuit in Fig. 6 is connected to it.

If the piezoelectric beam is not connected to any external circuits, which means neither D_1 nor D_2 is forward biased, the surface voltage on the piezoelectric beam at time t is

$$V_{\rm piezo}(t) = V_o(t) - V_o(t-\Delta t) + V_{\rm piezo}(t-\Delta t) \quad (1)$$

where $V_{\rm piezo}$ is the voltage on the piezoelectric beam, V_o is the input data from the open circuit measurement, and Δt is the time step in the finite-difference model.

If the piezoelectric beam is connected to the $C_{\rm load}$, which means D_1 is forward biased and D_2 is reverse biased, the surface voltage is

$$V_{\rm piezo}(t) = \frac{1}{2}(V_o(t) - V_o(t-\Delta t)) + V_{\rm piezo}(t-\Delta t). \quad (2)$$

If the piezoelectric beam makes D_2 forward biased, the surface voltage is

$$V_{\rm piezo}(t) = -V_{\rm th} \quad (3)$$

where $V_{\rm th}$ is the threshold voltage of the diode.

During the process, the load capacitor stays in two conditions. When D_1 is forward biased, the load capacitor extracts charge from the piezoelectric beam, so the voltage on the load capacitor at time t can be simulated as

$$V_{\rm load}(t) = V_{\rm piezo}(t) - V_{\rm th} \quad (4)$$

where $V_{\rm load}$ is the voltage on $C_{\rm load}$.

When D_1 is reverse biased, the voltage stays constant, so the voltage on $C_{\rm load}$ is

$$V_{\rm load}(t) = V_{\rm load}(t-\Delta t). \quad (5)$$

The piezoelectric model described above was coded in MATLAB and Fig. 9 presents the simulation results. The data of the open-circuit voltage was measured from the prototype, which is the same as the one shown in Fig. 5. According to the plots, the load capacitor extracts energy during the initial deflection of the beam and the first two positive vibrations, and the final amplitude of the voltage on $C_{\rm load}$ is 5.3 V.

Using the same analytical model, the prebiased case can be evaluated by reversing the polarity of the beam. In this case the input data is $-1 \times V_o(t)$, where $V_o(t)$ is the measured open-circuit voltage used in the unbiased case; the results are shown in Fig. 10. Most of the charge is extracted from the first positive peak to $C_{\rm load}$, when the beam starts to vibrate, and according to the simulation result, the voltage on $C_{\rm load}$ is 7.2 V.

By comparing the simulated results between the unbiased and prebiased cases, the output voltage is increased by 36%, which demonstrates that the prebiased case can dramatically improve the performance of the pulse generator.

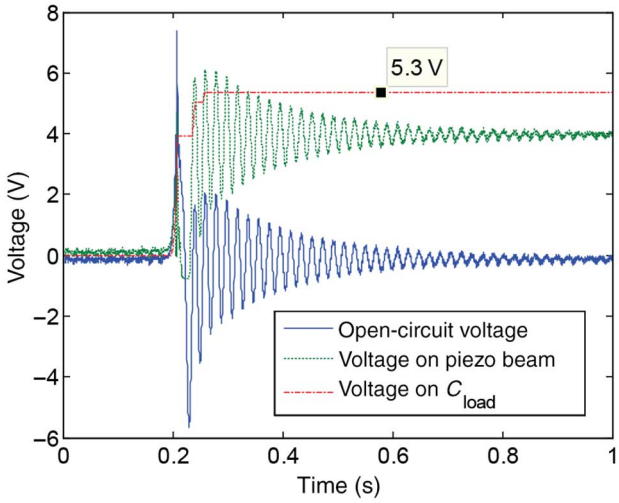

Fig. 9. Simulation result of the piezoelectric model.

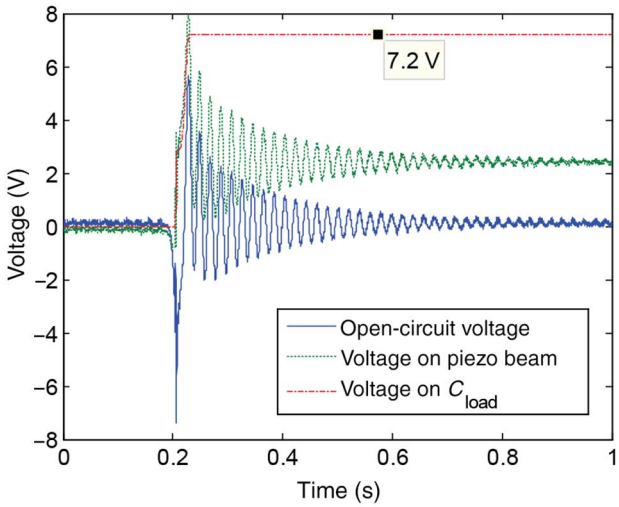

Fig. 10. Simulation result of the prebiased pulse generation.

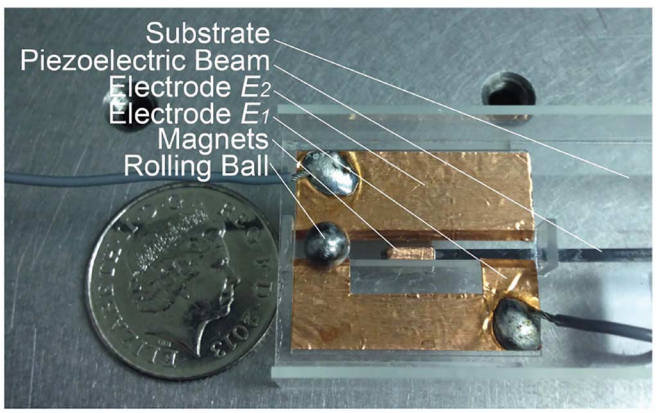

Fig. 11. Experimental model of the piezoelectric pulse generator.

B. Experimental Model and the Measurement Results

A centimetre scale pulse generator was built for experimental verification as shown in Fig. 11. A piezoelectric cantilever from Johnson Matthey is mounted under the substrate. The free length of the cantilever is 38 mm, which is the main factor to restrict the dimension of the device (75 mm × 27 mm × 25 mm). Two magnets (N45 neodymium) are chosen as the tip magnet for magnetic coupling and the dimensions are 5 mm × 1.5 mm × 1 mm for M_1 and 5 mm × 4 mm × 1.5 mm for M_2 as shown in Fig. 2. The capacitance of the piezoelectric beam is ∼10 nF for each of the piezoelectric layers and one layer is used in this prototype. The capacitance of the load capacitor is 10 nF to match the piezoelectric capacitance, and the two diodes D_1 and D_2 are both BAS45A low-leakage diodes. The electrodes E_1 and E_2 are made of copper tapes and attached through the V-groove track. The proof mass of the prototype is a 5 mm diameter steel ball, whose mass is ∼0.5 g. In the experiment, a resistor of 50 Ω is used as the load of the device.

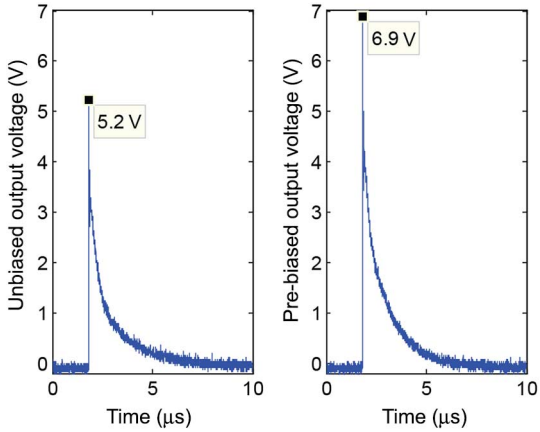

Fig. 12. Experimental results: output pulses generated with and without prebiased piezoelectric beam.

Fig. 12 illustrates the output voltages measured across the load resistor in the unbiased and prebiased cases, respectively. As shown in the plots, the load capacitor manages to extract the piezoelectric energy and store it for the next stage load circuit. The plots also demonstrate that the ball-electrodes switch can be used as self-synchronous switching for connection and disconnection between the pulse generator and the load when the device is operating. In addition, the output voltages are regulated to pulses via the intermediate circuit instead of resonant waveforms in Fig. 5.

As presented in Fig. 12, the amplitude of the pulse is 5.2 V in the unbiased case and 6.9 V in the prebiased case, and the voltage is increased by 33%, which indicates the validity of the simulation result.

Since the piezoelectric charges are stored in the load capacitor in each operating cycle, the energy per cycle can be evaluated as

$$E = \frac{1}{2} C_{\text{load}} V_{\text{load}}^2 \tag{6}$$

where E is the energy extracted in each cycle, C_{load} in use is 10 nF, and V_{load} is the amplitude of the pulses.

According to the measurements, the unbiased energy exacted per cycle is 135 nJ, and the prebiased energy per cycle is 238 nJ. This demonstrates that using the prebiased method, the energy extracted per pulse is increased by 76%. This pulse generator

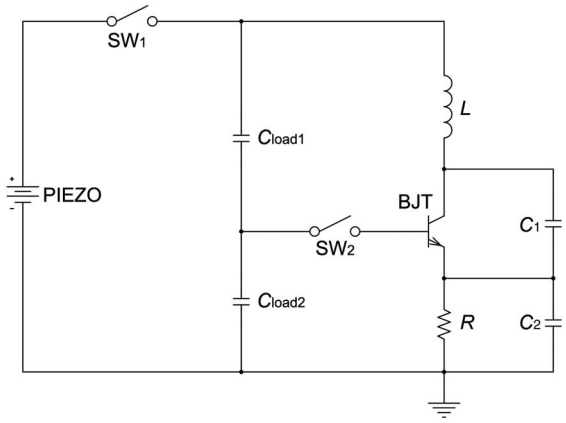

Fig. 13. Schematic of the pulse stimulated oscillator.

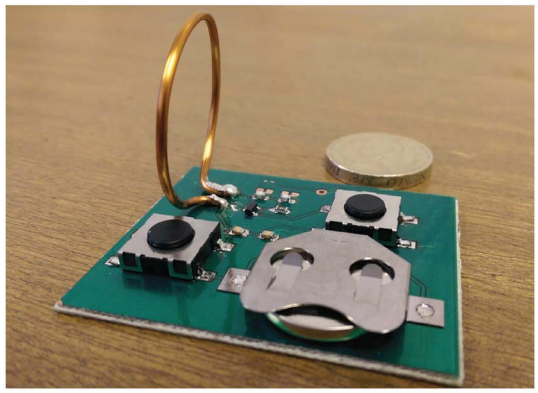

Fig. 14. Testing setup of the Colpitts oscillator.

TABLE I
PARAMETERS OF THE TESTING CIRCUIT

Component	Part number/value	Component	Part number/value
V_{PIEZO}	3 V	R	1 kΩ
C_{load1}	22 nF	C_1	1 pF
C_{load2}	22 nF	C_2	1 pF
L	58 nH	BJT	BFR35AP

can achieve its function by combining physical contacts as a mechanical switch and diodes as an electric switch. But it is worth pointing out that the physical contacts made by the steel ball and the copper tapes may inject noise to the output of the pulse generator due to the dynamic contact resistance when the ball is traveling. In addition, the deformation of the piezoelectric beam may result in slight change of the piezoelectric capacitance, which may also influence the charge sharing process between the load capacitor and the piezoelectric capacitor.

V. Transmitter Circuit Design

Since the prototype can generate a fixed amount of energy in each operating cycle, it is possible to apply this pulse generator to a wireless sensing device. Unlike a dc power source, such as a battery, it can only supply discrete power to the load circuit. Considering the particular design and taking advantage of this impulse mechanism, an oscillation circuit can be used as a load transmitter for the pulse generator.

A. Pulse-Stimulated Colpitts Oscillator

A pulse-stimulated Colpitts oscillator was designed based on the circuits proposed in [16] and [17] as a low power transmitter for wireless sensing.

Fig. 13 presents the schematic of the oscillation circuit. The piezoelectric pulse generator is replaced with a dc power source V_{PIEZO} to simplify the testing. The switch SW_1 is applied to control the connection and disconnection between the dc power source and its load. Instead of a single load capacitor in the pulse generator, this circuit requires two capacitors C_{load1} and C_{load2} in series to provide a bias voltage for the bipolar transistor (BJT). Switch SW_2 represents the ball-electrodes mechanical switch in the pulse generator. The right-hand side of the circuit in Fig. 13 is the oscillator. Inductor L represents the antenna for the transmitter, and forms an LC tank with the two capacitors C_1 and C_2. The npn-type BJT is a high-frequency BJT and the resistor R is used to control the power consumption.

The testing circuit setup is illustrated in Fig. 14. In this circuit, a loop antenna, which is made of a 1.5-mm-diameter copper wire, is used, and the diameter of the antenna is 30 mm. The inductance of a loop wire can be estimated as [18]

$$L \approx \mu_o \mu_r \frac{D}{2}\left[\ln\left(\frac{8D}{d}\right) - 2\right] \tag{7}$$

where L is the inductance of the loop antenna, μ_o is the permeability of free space, μ_r is the relative permeability of the medium, which is approximately 1 for copper, D is the diameter of the loop, and d is the diameter of the wire. The inductance of the loop antenna can thus be estimated as 58 nH. A coin cell battery of 3 V is used to represent the energy from the piezoelectric beam and two push-button switches are used to control the circuit as shown in Figs. 13 and 14. In this circuit, the mechanical switch SW_2 is connected between the two load capacitors, which leaves C_{load1} directly connected to the transmitter. This change does not cause the load capacitors to discharge before SW_2 is closed, because the BJT is OFF without the bias voltage at the base, and in this case, the collector stops current flowing to the emitter. The parameters of the components on the testing board are listed in Table I.

In the test, a loop antenna of the same size as the one for the transmitter is used to receive the transmitted signal, and is directly connected to an oscilloscope for measurement. For each of the operating cycles, SW_1 is closed first to allow the two load capacitors to be charged by the battery. After the charge, SW_1 turns OFF and SW_2 is closed to provide the bias voltage to the base of the BJT. In this case, the BJT starts to operate, which is powered by the two load capacitors. After the energy stored in C_{load1} and C_{load2} is dissipated by the transmitter, the circuit stops working.

Fig. 15 shows the received signal in one operating cycle. The received signal shows a continuous decrease in voltage. This happens since the power is from the discharge of the two load

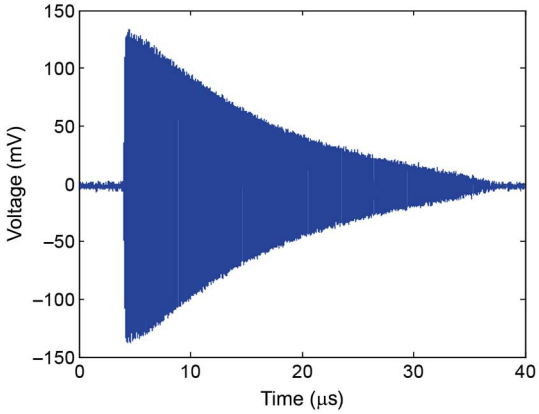

Fig. 15. Transient measurement of the received signal for one operating cycle.

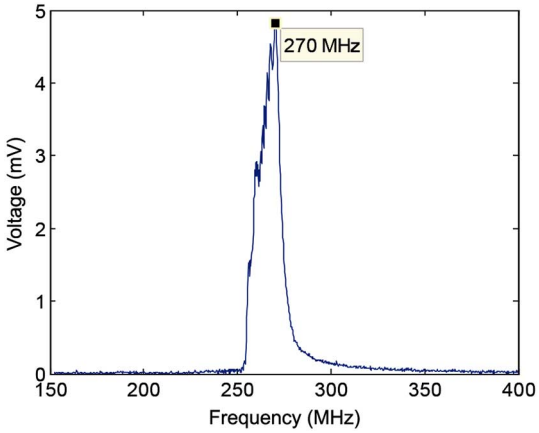

Fig. 16. Frequency analysis of the transmitted signal.

capacitors, and the voltage across the oscillator decreases with the discharge. The time constant of the prototype is

$$\tau = R\left(\frac{C_{\text{load1}}C_{\text{load2}}}{C_{\text{load1}}+C_{\text{load2}}}\right) \tag{8}$$

where R is $1\,\text{k}\Omega$, and C_{load1} and C_{load2} are both 22 nF according to Table I. Therefore, the theoretical time constant of the circuit is $11\,\mu\text{s}$, whereas the measured time constant is approximately $13\,\mu\text{s}$ in Fig. 15 using curve fitting, which is very close.

A frequency analysis of the transmitted signal is presented in Fig. 16. Due to the continuous discharge of the load capacitors, the voltage across the BJT decreases. In this case, the capacitance of the transistor is changed and so does the resonant frequency of the oscillator, which causes the frequency of the signal shift from 270 to 250 MHz. The plot shows an asymmetric frequency spectrum, and the received amplitude decays with the decrease in frequency, which is because with lower voltage applied to the oscillator, the resonant frequency of the circuit decreases accordingly.

The experimental result demonstrates that the oscillator can be discretely powered by the energy stored in capacitors. However, the drawback of the design is the changes in the signal amplitude and frequency. In order to detect a signal from a sensor, such as the pH sensor in [19], a sensor input must be

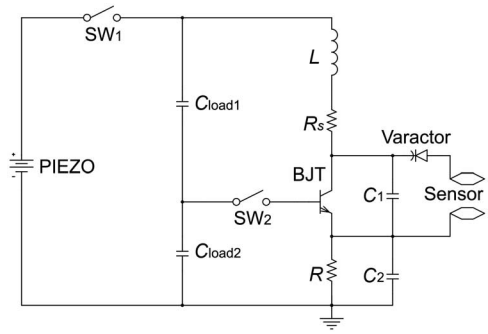

Fig. 17. Schematic of the FM transmitter for the piezoelectric generator.

installed to the circuit. An amplitude modulation method to process the sensor signal has been presented in [20]. However, in terms of wireless sensing, the AM-based transmission is susceptible to the noise from the environment, which makes it difficult for the receiver to filter out the signal. In addition, the amplitude of the received signal varies with the changes in transmission distance and direction, and so requires references to calibrate the signal during demodulation. There are many different modulation techniques for wireless sensing, such as phase-shift keying, frequency-shift keying, and quadrature amplitude modulation [21], but these digital modulation techniques requires more complicated architecture, which is not suitable for the case that only one impulse power is provided. Therefore, with the given pulse generator as the only power source, an approach using frequency modulation is considered most suitable.

B. FM-Based Transmission

In order to implement a frequency modulation approach to the transmitter, a varactor is connected between the transmitter and the output of the sensor to form a voltage-controlled oscillator as shown in Fig. 17. Each time after the load capacitors are charged and SW_2 is closed, a signal is transmitted, with frequency range decided by the LC tank and the voltage from the sensor. In the simulation, the discharge time of the load capacitors is set at $10\,\mu s$ for a clearer demonstration. It is necessary to point out that setting the discharge time is not required for the real transmitter, because different frequency ranges can be detected even if there is overlapping between them. In this design, the minimum step of the sensor voltage is set at 0.1 V. Since the entire discharge time is very short ($\ll$1 ms) according to Fig. 15, the output of the sensor can be assumed constant in each operating cycle. This assumption defines the operating principle of the FM transmitter: in each operating cycle, the device transmitted the instant signal to the receiver, and if the frequency range of the received signal changes in one cycle, it indicates the sensing condition changes, and can be detected by the receiver. Table II gives the parameters of the FM transmitter design and Fig. 18 is the transient analysis of the FM transmitter.

When the switch SW_2 is closed, the LC tank oscillates at the frequency decided by the sensor voltage for $10\,\mu\text{s}$ in each operating cycle. The frequency analysis of the current through the antenna L is illustrated in Fig. 19 with sensor voltage trimmable

TABLE II
PARAMETERS OF THE FM TRANSMITTER CIRCUIT

Component	Part number/value	Component	Part number/value
V_{PIEZO}	6 V	R	10 kΩ
C_{load1}	30 nF	C_1	1 pF
C_{load2}	15 nF	C_2	12 pF
L	100 nH	Varactor	BBY52-02w
R_s	1.36 Ω	V_{Sensor}	−0.2 to 0.2 V
BJT	MMBR931		0.1 V step

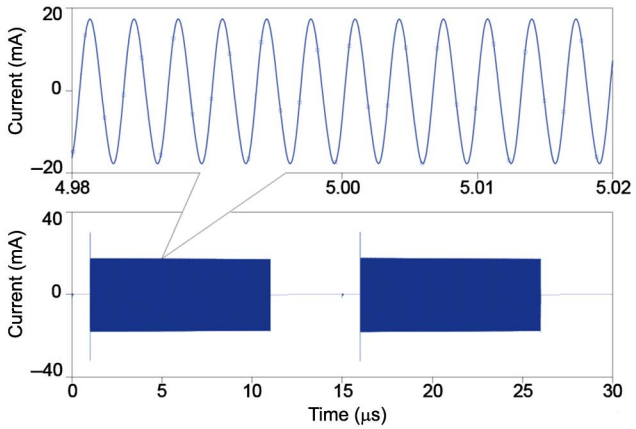

Fig. 18. Transient analysis of the FM transmitter by OrCAD ($V_{\mathrm{Sensor}} = 0.1$ V).

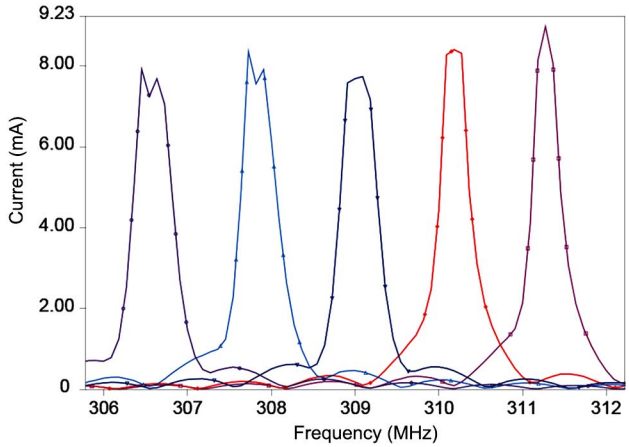

Fig. 19. Frequency analysis of the transmitter by OrCAD: with V_{Sensor} increases from −0.2 to 0.2 V (0.1 V steps), the resonant frequency decreases.

from −0.2 to 0.2 V. As can be seen from the analysis result, the operating frequency of the FM transmitter varies between 306 and 312 MHz. The result provides good linearity between the operating frequency and the sensor voltage. This proves that the operating frequency of the FM transmitter can be linearly controlled by the change in the sensor voltage, and the signal from the sensor can be modulated in the frequency domain by the transmitter.

VI. CONCLUSION

A rolling ball pulse generator has been presented in this paper using piezoelectric transduction for wireless sensing. Both simulation and experiment results are illustrated to demonstrate the operating principle and feasibility of this device. A passive prebias mechanism is introduced to enhance the performance of the piezoelectric pulse generator, and it was demonstrated both by simulation and experiment that the prebias method can extract 76% more energy from the device compared to the unbiased case. This result is expected to enhance the energy density of low-frequency and impulse-excited piezoelectric harvesting devices. The simulation results of the piezoelectric pulse generator are consistent with the experimental results. However, this analytical method ignores the mutual influence between the electrical changes and the mechanical changes of the piezoelectric beam, and a simulation model is under development by exploring a more comprehensive relationship between the tip displacement of the piezoelectric beam and the voltage generated.

An oscillation circuit based on a Colpitts oscillator was built to test the design when the oscillator is powered by discontinuous energy from load capacitors. The result shows promising performance as the energy from the load capacitors can be successfully transmitted to the receiver. This device could be adapted to any miniature passive sensor having a voltage output in a suitable range, such as the pH sensor in [19], thermopiles, piezoelectric strain sensors, etc. The simulation results prove that the signal from a sensor can be modulated in the frequency domain by the capacitor-powered oscillator, which demonstrates the feasibility of the proof-of-concept wireless sensing prototype based on the piezoelectric pulse generator.

REFERENCES

[1] G.-Z. Yang and M. Yacoub, *Body Sensor Networks*, 2nd ed. New York, NY, USA: Springer, 2014.
[2] O. E. Semonin *et al.*, "Peak external photocurrent quantum efficiency exceeding 100% via MEG in a quantum dot solar cell," *Science*, vol. 334, no. 6062, pp. 1530–1533, 2011.
[3] Y. Li, K. Buddharaju, N. Singh, G. Lo, and S. Lee, "Chip-level thermoelectric power generators based on high-density silicon nanowire array prepared with top-down CMOS technology," *IEEE Electron Device Lett.*, vol. 32, no. 5, pp. 674–676, May 2011.
[4] P. D. Mitcheson, E. M. Yeatman, G. K. Rao, A. S. Holmes, and T. C. Green, "Energy harvesting from human and machine motion for wireless electronic devices," *Proc. IEEE*, vol. 96, no. 9, pp. 1457–1486, Sep. 2008.
[5] C. He, M. E. Kiziroglou, D. C. Yates, and E. M. Yeatman, "A MEMS self-powered sensor and RF transmission platform for WSN nodes," *IEEE Sensors J.*, vol. 11, no. 12, pp. 3437–3445, Dec. 2011.
[6] K. Cook-Chennault, N. Thambi, and A. Sastry, "Powering MEMS portable devices—A review of non-regenerative and regenerative power supply systems with special emphasis on piezoelectric energy harvesting systems," *Smart Mater. Struct.*, vol. 17, no. 4, p. 043001, 2008.
[7] E. Aktakka, R. Peterson, and K. Najafi, "Thinned-PZT on SOI process and design optimization for piezoelectric inertial energy harvesting," in *Proc. IEEE Solid-State Sens. Actuators Microsyst. Conf. (TRANSDUCERS)*, 2011, pp. 1649–1652.
[8] Y. Minami and E. Nakamachi, "Development of enhanced piezoelectric energy harvester induced by human motion," in *Proc. Annu. Int. Conf. IEEE Eng. Med. Biol. Soc. (EMBC)*, 2012, pp. 1627–1630.
[9] P. Pillatsch, E. M. Yeatman, and A. S. Holmes, "A scalable piezoelectric impulse-excited generator for random low frequency excitation," in *Proc. 25th IEEE Int. Conf. Micro Electro Mech. Syst. (MEMS)*, 2012, pp. 1205–1208.
[10] A. Erturk and D. J. Inman, *Piezoelectric Energy Harvesting*. Hoboken, NJ, USA: Wiley, 2011.
[11] J. Dicken, P. D. Mitcheson, I. Stoianov, and E. M. Yeatman, "Increased power output from piezoelectric energy harvesters by pre-biasing," in *Proc. PowerMEMS*, 2009, pp. 1–4.

[12] D. Zhu *et al.*, "A novel piezoelectric energy harvester designed for single-supply pre-biasing circuit," *J. Phys.*, vol. 476, no. 1, p. 012134, 2013.
[13] N. G. Elvin and A. A. Elvin, "A general equivalent circuit model for piezoelectric generators," *J. Intell. Mater. Syst. Struct.*, vol. 20, no. 1, pp. 3–9, 2009.
[14] J. Ajitsaria, S.-Y. Choe, D. Shen, and D. Kim, "Modeling and analysis of a bimorph piezoelectric cantilever beam for voltage generation," *Smart Mater. Struct.*, vol. 16, no. 2, p. 447, 2007.
[15] B. Richter, J. Twiefel, and J. Wallaschek, "Piezoelectric equivalent circuit models," in *Energy Harvesting Technologies*. New York, NY, USA: Springer, 2009, pp. 107–128.
[16] B. Ziaie, K. Najafi, and D. J. Anderson, "A low-power miniature transmitter using a low-loss silicon platform for biotelemetry," in *Proc. 19th Annu. Int. Conf. IEEE Eng. Med. Biol. Soc.*, vol. 5. Piscataway, NJ, USA: IEEE, 1997, pp. 2221–2224.
[17] D. C. Yates, A. S. Holmes, and A. J. Burdett, "Optimal transmission frequency for ultralow-power short-range radio links," *IEEE Trans. Circuits Syst. I. Reg. Pap.*, vol. 51, no. 7, pp. 1405–1413, 2004.
[18] C. A. Balanis, *Antenna Theory: Analysis and Design*. Hoboken, NJ, USA: Wiley, 2012.
[19] E. Bitziou, D. O'Hare, and B. A. Patel, "Simultaneous detection of pH changes and histamine release from oxyntic glands in isolated stomach," *Anal. Chem.*, vol. 80, no. 22, pp. 8733–8740, 2008.
[20] H. Jiang and E. M. Yeatman, "A piezoelectric pulse generator for low frequency non-harmonic vibration," *J. Phys.*, vol. 476, no. 1, p. 012059, 2013.
[21] M. S. Dawood, "A survey on energy efficient modulation and coding techniques for wireless sensor networks," *J. Global Res. Comput. Sci.*, vol. 4, no. 1, pp. 63–66, 2013.

Hao Jiang received the B.Eng. degree from the Dalian University of Technology, Dalian, China, in 2010, the M.Sc. degree from Imperial College London, London, U.K., in 2011, and is currently working toward the Ph.D. degree at Imperial College London.

He is currently with the Optical and Semiconductor Devices Group, Department of Electrical and Electronic Engineering, Imperial College London. His research interests include microelectromechanical systems and energy harvesting for wireless sensor network nodes.

Michail E. Kiziroglou (M'04) received the Diploma degree in electrical and computer engineering from the Aristotle University of Thessaloniki, Thessaloniki, Greece, in 2000, the Master's degree in microelectronics and nanoelectronics from the Democritus University of Thrace, Xanthi, Greece, in 2003, and the Ph.D. degree in microelectronics and spintronics from the University of Southampton, Southampton, U.K., in 2007.

He is currently a Researcher with the Optical and Semiconductor Devices Group, Imperial College London, London, U.K. His research interests include energy harvesting devices, microengineering, and energy autonomous wireless sensors.

David C. Yates (M'03) received the M.Eng. degree in electrical engineering and Ph.D. degree in ultralow-power wireless links from Imperial College London, London, U.K., in 2001 and 2007, respectively.

He is currently a Research Fellow with the Control and Power Group, Department of Electrical and Electronic Engineering, Imperial College London. His research interests include wireless power and ultralow power RF, and analog circuits for sensor networks.

Eric M. Yeatman (M'01–SM'05–F'13) received the B.Sc. degree from Dalhousie University, Halifax, NS, Canada, in 1983, and the Ph.D. degree from Imperial College London, London, U.K., in 1989.

Since 1989, he has been a Member of Academic Staff with the Department of Electrical and Electronic Engineering, Imperial College London, where he is currently a Professor of microengineering and Deputy Head of the Department of Electrical and Electronic Engineering. His research interests include micromechanical actuators and generators, microstructures for optical and RF applications, and technologies for pervasive sensing.